

Enhancement of image resolution beyond the diffraction limit by double dark resonancesOnkar N. Verma^{*} and Tarak N. Dey[†]*Department of Physics, Indian Institute of Technology Guwahati, Guwahati- 781 039, Assam, India*

(Received 15 November 2013; published 17 March 2014)

We show how quantum coherence effects can be used to improve the resolution and the contrast of diffraction-limited images imprinted onto a probe field. The narrow and sharp spectral features generated by double dark resonances (DDR) are exploited to control absorption, dispersion, and diffraction properties of the medium. The spatially modulated control field can produce inhomogeneous susceptibility of the medium that encodes the spatial feature of the control image to probe field in the presence of DDR. The transmission of a cloned image can be enhanced by the use of an incoherent pump field. We find that the feature size of the cloned image is four times smaller than the initial characteristic size of the control image even though the control image is completely distorted after propagation through a 3-cm-long Rb vapor cell. We further discuss how spatial optical switching is possible by using induced transparency and absorption of the medium.

DOI: [10.1103/PhysRevA.89.033830](https://doi.org/10.1103/PhysRevA.89.033830)

PACS number(s): 42.30.-d, 42.50.Gy, 32.80.Qk, 42.65.-k

I. INTRODUCTION

The ability to enhance spatial resolution of a Rayleigh or Sparrow limited image is one of the main challenges in optics [1]. Conventional optics has failed to resolve the characteristic size of an image beyond a value comparable to the wavelength of the probing light [2]. The main constraint of high-resolution imaging comes from diffraction and absorption. The diffraction of an image is inevitable due to its geometrical origin [3]. The above obstacles can be completely or partially eliminated by use of quantum interference effects.

Coherent electromagnetic fields interacting in a multilevel atomic system induce atomic coherence. The induced atomic coherence can be exploited to demonstrate many interesting phenomena such as coherent population trapping (CPT) [4], electromagnetically induced transparency (EIT) [5,6], lasing without inversion (LWI) [7], and saturated absorption techniques [8,9]. A suitable spatially dependent profile of the control field can produce a waveguidelike structure inside the medium which controls image propagation without diffraction [10–13]. This spatially varying refractive index can also guide focusing [14–18], defocusing [19], self-imaging [20], and steering of the probe beam [21,22]. Most of the schemes employ a spatially inhomogeneous control field to protect the image from diffraction. In a different development, Firstenberg *et al.* theoretically and experimentally found that Dicke narrowing by atomic motion and velocity-changing collisions is useful to eliminate the diffraction of an arbitrary image [23–25].

Tailoring the optical properties of the medium along the transverse direction can open up a new possibility of transferring the characteristic features of the control field to the probe field. This is because the propagation dynamics of the probe field is dependent on the diffraction and dispersive properties of the medium. The diffraction and dispersion characteristics of the atomic medium can be manipulated by using a proper spatially inhomogeneous control field. This concept has been demonstrated both experimentally [26] and

theoretically [27] in a CPT system where a well resolved control field structure is used for optical cloning. Further, the transmitted cloned image has a feature size four times smaller as compared to the initial control image. However, all of these schemes suffer from strong absorption due to breaking of the two-photon resonance condition. Hence the absorption-based mechanism limits practical implementation. Therefore, one can take advantage of gain-based schemes to generate a high-resolution cloned image. The resolution of the cloned image can be improved by engineering the contrast of the refractive index of atomic waveguides of the gain medium. Quantum interference effects induced by interacting dark resonances have been shown to drastically increase the contrast of the refractive index profile [28,29].

In this paper, we have used double dark resonances to imprint the Rayleigh-limited or Sparrow-limited control image to probe field with high resolution and contrast. To facilitate these processes, we use a four-level atomic system. A single dark state can be created by the control and the probe fields coupling to the two arms of a Λ system. This interaction gives rise to a usual single transparency window. The double dark states can be generated by using a microwave or optical field which interacts with magnetic or electric dipole moments of relevant atomic transitions [30–32]. We find that the interference between two dark states results in a new sharp absorption peak at line center. The DDR spectra show two transparency windows accompanied with one sharp absorption peak. Furthermore, we demonstrated that a very weak incoherent pump field is sufficient to turn the induced absorption dips into gain peaks. We exploit these sharp spectral features to write a waveguide inside the medium. We begin with a Rayleigh-limited control field structure and do a comparative study of inhomogeneous susceptibility for EIT, microwave-induced absorption (MIA), and LWI. The result shows that the presence of three fields with an incoherent pump provides a sharp contrast in refractive index from core to cladding than the other two cases. We efficiently use this sharp refractive index contrast for cloning the Rayleigh-limited control field image to the probe field with high resolution. Finally, we also show that the Sparrow-limited three modes of the control image can also be cast onto the probe field with appreciable resolution and high transmission. Later, we

^{*}onkar@iitg.ernet.in[†]tarak.dey@gmail.com

also use induced absorption and a transparency mechanism to demonstrate the spatial switching (off or on) of a probe beam. The spatial optical beam switching based on spatial phase modulation has been discussed recently in optical lattices [33].

The organization of the paper is as follows. In the next section, we introduce our model configuration, discuss the equations of motion for a four-level system, describe the perturbative analysis of linear susceptibility of the probe field, and derive the beam propagation equations for both probe and control fields under paraxial approximations. In Sec. III, we present our results. First, we describe the linear response of the medium to the probe field under the action of the spatially independent as well as the spatially dependent control beam. We then employ the spatial dependent susceptibility to explain the basic principle of cloning of a Rayleigh-limited control image to the probe field with high resolution and high contrast. Next we provide numerical results on the propagation dynamics of cloned images with different spatial structure of the control fields for the LWI, EIT, and MIA cases. Section IV provides a summary and discussion of our results.

II. THEORETICAL FORMULATIONS

A. Model configuration

In this work, we consider a homogeneously broadened four-level atomic system consisting of an excited state $|4\rangle$ and three metastable states $|1\rangle$, $|2\rangle$, and $|3\rangle$ interacting with two optical fields and one microwave field as shown in Fig. 1. The excited state $|4\rangle$ is coupled to two degenerate ground states $|1\rangle$ and $|3\rangle$ by two coherent fields, namely, a weak probe field with frequency ω_1 and a control field with frequency ω_2 , respectively, which forms a three-level Λ system. The ground state $|3\rangle$ is further coupled to the metastable state $|2\rangle$ by an additional microwave field with frequency ω_3 . The proposed scheme can be realized in ^{87}Rb atoms which contain ground levels $|1\rangle = |5S_{1/2}, F = 2, m = 2\rangle$, $|2\rangle = |5S_{1/2},$

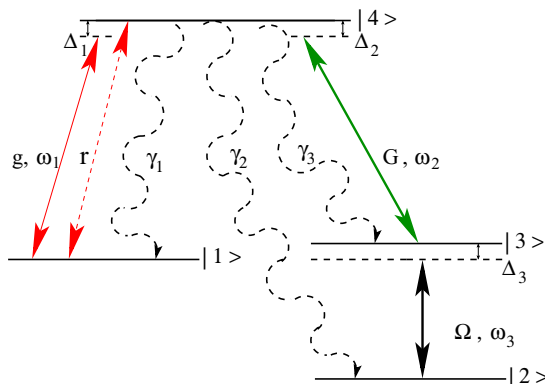


FIG. 1. (Color online) Schematic diagram of the four-level ^{87}Rb atomic system. The atomic transition $|4\rangle \leftrightarrow |1\rangle$ is coupled by the coherent probe field g and incoherent pump field r . The control field G interacts with the atomic transition $|4\rangle \leftrightarrow |3\rangle$. A microwave field Ω acts on the transition $|3\rangle \leftrightarrow |2\rangle$ to produce the double dark resonance of the system.

$F = 1, m = 0\rangle$, and $|3\rangle = |5S_{1/2}, F = 2, m = 0\rangle$ and the excited level $|4\rangle = |5P_{3/2}, F' = 2, m = 1\rangle$ [30,31]. We define two copropagating optical fields along the z axis as

$$\vec{E}_j(\vec{r}, t) = \hat{e}_j \mathcal{E}_j(\vec{r}) e^{-i(\omega_j t - k_j z)} + \text{c.c.}, \quad (1)$$

where $\mathcal{E}_j(\vec{r})$ is the slowly varying envelope, \hat{e}_j is the unit polarization vector, ω_j is the laser field frequency, and k_j is the wave number of the field, respectively. The index $j \in \{1, 2\}$ denotes the probe or control field, respectively. The microwave field is defined as

$$\vec{E}_3(r, t) = \hat{e}_3 \mathcal{E}_3(\vec{r}) e^{-i(\omega_3 t - k_3 z)} + \text{c.c.}, \quad (2)$$

where $\mathcal{E}_3(\vec{r})$ is constant amplitude and ω_3 is the frequency of the microwave field. In the presence of three coherent fields, the Hamiltonian of the system under the electric dipole and rotating-wave approximation can be expressed as

$$H = H_0 + H_I, \quad (3a)$$

$$H_0 = \hbar\omega_{43}|4\rangle\langle 4| - \hbar\omega_{23}|2\rangle\langle 2| - \hbar\omega_{13}|1\rangle\langle 1|, \quad (3b)$$

$$H_I = -(|4\rangle\langle 1|\mathbf{d}_{41} \cdot \mathcal{E}_1 e^{-i(\omega_1 t - k_1 z)} + |4\rangle\langle 3|\mathbf{d}_{43} \cdot \mathcal{E}_2 e^{-i(\omega_2 t - k_2 z)} + |3\rangle\langle 2|\mathbf{d}_{32} \cdot \mathcal{E}_3 e^{-i(\omega_3 t - k_3 z)} + \text{H.c.}). \quad (3c)$$

The time dependent parts of the above Hamiltonian can be removed by use of unitary transformation,

$$W = e^{-(i/\hbar)U t}, \quad (4a)$$

$$U = \hbar\omega_2|4\rangle\langle 4| - \hbar\omega_3|2\rangle\langle 2| - \hbar(\omega_1 - \omega_2)|1\rangle\langle 1|. \quad (4b)$$

Now, we can rewrite the transformed Hamiltonian as

$$V/\hbar = -\Delta_2|4\rangle\langle 4| + \Delta_3|2\rangle\langle 2| + (\Delta_1 - \Delta_2)|1\rangle\langle 1| - (g|4\rangle\langle 1| + G|4\rangle\langle 3| + \Omega|3\rangle\langle 2| + \text{H.c.}), \quad (5)$$

where $\Delta_1 = \omega_1 - \omega_{41}$, $\Delta_2 = \omega_2 - \omega_{43}$, and $\Delta_3 = \omega_3 - \omega_{32}$ are the single-photon detunings and

$$g = \frac{\vec{d}_{41} \cdot \vec{\mathcal{E}}_1 e^{ik_1 z}}{\hbar}, \quad G = \frac{\vec{d}_{43} \cdot \vec{\mathcal{E}}_2 e^{ik_2 z}}{\hbar}, \quad \Omega = \frac{\vec{d}_{32} \cdot \vec{\mathcal{E}}_3 e^{ik_3 z}}{\hbar}$$

are the Rabi frequencies of the probe, control, and microwave fields, respectively. The atomic transition frequencies and the corresponding dipole moment matrix elements are denoted by ω_{ij} and \vec{d}_{ij} , respectively.

B. Dynamical equations

We use Liouville's equation to incorporate the coherent and incoherent processes of the atomic system. Thus the dynamics of the system are governed by the following Liouville equation:

$$\dot{\rho} = -\frac{i}{\hbar}[V, \rho] + \mathcal{L}\rho, \quad (6)$$

where the second term represents the incoherent processes that can be determined by

$$\mathcal{L}\rho = \mathcal{L}_\gamma \rho + \mathcal{L}_d \rho + \mathcal{L}_r \rho, \quad (7)$$

with

$$\begin{aligned}\mathcal{L}_\gamma\rho &= -\sum_{i=1}^3\frac{\gamma_i}{2}(|4\rangle\langle 4|\rho - 2|i\rangle\langle i|\rho_{44} + \rho|4\rangle\langle 4|), \\ \mathcal{L}_d\rho &= -\sum_{i=1}^3\sum_{i\neq j=1}^3\frac{\gamma_c}{2}(|i\rangle\langle i|\rho - 2|j\rangle\langle j|\rho_{ii} + \rho|i\rangle\langle i|), \\ \mathcal{L}_r\rho &= \mathcal{L}_{14}\rho + \mathcal{L}_{41}\rho, \\ \mathcal{L}_{14}\rho &= -\frac{r}{2}(|4\rangle\langle 4|\rho - 2|1\rangle\langle 1|\rho_{44} + \rho|4\rangle\langle 4|), \\ \mathcal{L}_{41}\rho &= -\frac{r}{2}(|1\rangle\langle 1|\rho - 2|4\rangle\langle 4|\rho_{11} + \rho|1\rangle\langle 1|).\end{aligned}$$

The first term of Eq. (7) refers to the radiative decay from excited state $|4\rangle$ to ground states $|j\rangle$ as labeled by γ_j . The second term, $\mathcal{L}_d\rho$, represents pure dephasing for the coherence ρ_{ij} due to collision at a rate γ_c . The incoherent pumping between levels $|1\rangle$ and $|4\rangle$ with a rate r is given by $\mathcal{L}_r\rho$. The dynamics of the population and atomic coherences in the four-level system can be described by the following set of density matrix equations:

$$\dot{\rho}_{11} = -r\rho_{11} + r\rho_{44} + \gamma_1\rho_{44} + ig^*\rho_{41} - ig\rho_{14}, \quad (8a)$$

$$\dot{\rho}_{22} = \gamma_2\rho_{44} + i\Omega^*\rho_{32} - i\Omega\rho_{23}, \quad (8b)$$

$$\dot{\rho}_{33} = \gamma_3\rho_{44} + i\Omega\rho_{23} - i\Omega^*\rho_{32} + iG^*\rho_{43} - iG\rho_{34}, \quad (8c)$$

$$\dot{\rho}_{44} = -\dot{\rho}_{11} - \dot{\rho}_{22} - \dot{\rho}_{33}, \quad (8d)$$

$$\begin{aligned}\dot{\rho}_{21} &= -\left[\frac{r}{2} + \gamma_{21} - i(\Delta_1 - \Delta_2 - \Delta_3)\right]\rho_{21} \\ &\quad + i\Omega^*\rho_{31} - ig\rho_{24},\end{aligned} \quad (8e)$$

$$\dot{\rho}_{23} = -[\gamma_{23} + i\Delta_3]\rho_{23} - iG\rho_{24} + i\Omega^*(\rho_{33} - \rho_{22}), \quad (8f)$$

$$\begin{aligned}\dot{\rho}_{24} &= -[\gamma_{24} + i(\Delta_2 + \Delta_3)]\rho_{24} - ig^*\rho_{21} \\ &\quad - iG^*\rho_{23} + i\Omega^*\rho_{34},\end{aligned} \quad (8g)$$

$$\begin{aligned}\dot{\rho}_{31} &= -\left[\frac{r}{2} + \gamma_{31} + i(\Delta_2 - \Delta_1)\right]\rho_{31} + i\Omega\rho_{21} - ig\rho_{34} \\ &\quad + iG^*\rho_{41},\end{aligned} \quad (8h)$$

$$\begin{aligned}\dot{\rho}_{34} &= -[\gamma_{34} + i\Delta_2]\rho_{34} - ig^*\rho_{31} + i\Omega\rho_{24} \\ &\quad - iG^*(\rho_{33} - \rho_{44}),\end{aligned} \quad (8i)$$

$$\begin{aligned}\dot{\rho}_{41} &= -\left[\frac{r}{2} + \gamma_{41} - i\Delta_1\right]\rho_{41} + iG\rho_{31} + ig(\rho_{11} - \rho_{44}), \\ &\quad (8j)\end{aligned}$$

$$\dot{\rho}_{ij} = \dot{\rho}_{ji}^*, \quad (8k)$$

where the overdots stand for time derivatives and “*” denotes complex conjugate. The total dephasing rate of the atomic coherences is given by $\gamma_{ij} = \gamma_c + \gamma_i/2$.

C. Perturbative analysis

We adopt steady-state solutions of the master equations (8) to study the response of the medium. The equations (8) can be solved to all orders in the control and probe fields provided both the fields have approximately equal amplitude [27]. However, in the context of a weak probe field limit, we calculate the

coherences and populations to the first order in g and to all orders in control field G and microwave field Ω . Hence the steady-state solutions of the density-matrix equations can be written in the form

$$\rho_{ij} = \rho_{ij}^{(0)} + g\rho_{ij}^{(+)} + g^*\rho_{ij}^{(-)}, \quad (9)$$

where $\rho_{ij}^{(0)}$ describes the solution in the absence of the probe field. The second and third terms denote the solutions at positive and negative frequencies of the probe field, respectively. We now substitute the above expression in Eqs. (8) and equate the coefficients of g , g^* and the constant terms. Thus, we obtain a set of 16 coupled simultaneous equations. The solutions of simultaneous equations which are relevant for susceptibility expression are given in the Appendix. Now, the steady-state value of the atomic coherence $\rho_{41}^{(+)}$ will yield a susceptibility χ_{41} at frequency ω_1 ,

$$\rho_{41}^{(+)} = i\left(\frac{(\Gamma_{21}\Gamma_{31} + \Omega^2)(\rho_{11}^{(0)} - \rho_{44}^{(0)}) + A|G|^2}{\Gamma_{41}(\Gamma_{21}\Gamma_{31} + \Omega^2) + \Gamma_{21}|G|^2}\right), \quad (10)$$

with

$$A = \frac{B(\rho_{44}^{(0)} - \rho_{33}^{(0)}) + C(\rho_{33}^{(0)} - \rho_{22}^{(0)})}{[\Gamma_{23}(\Gamma_{24}\Gamma_{34} + \Omega^2) + \Gamma_{34}|G|^2]},$$

$$B = [\Gamma_{21}(\Gamma_{23}\Gamma_{24} + |G|^2) - \Gamma_{23}\Omega^2],$$

$$C = (\Gamma_{21} + \Gamma_{34})\Omega^2,$$

where $\Gamma_{21} = [r/2 + \gamma_{21} - i(\Delta_1 - \Delta_2 - \Delta_3)]$, $\Gamma_{23} = [\gamma_{23} + i\Delta_3]$, $\Gamma_{24} = [\gamma_{24} + i(\Delta_2 + \Delta_3)]$, $\Gamma_{31} = [r/2 + \gamma_{31} + i(\Delta_2 - \Delta_1)]$, $\Gamma_{34} = [\gamma_{34} - i\Delta_2]$, and $\Gamma_{41} = [r/2 + \gamma_{41} - i\Delta_1]$. For simplicity, we have assumed equal decay rates from excited state, $\gamma_1 = \gamma_2 = \gamma_3 = \gamma$, and coherence dephasing rates $\gamma_{41} = \gamma_{24} = \gamma_{34} \approx \gamma$, $\gamma_{21} = \gamma_{31} = \gamma_{23} \approx \gamma_c = \Gamma$. We now express the macroscopic polarization of the medium in terms of both the atomic coherences as well as the susceptibility as

$$\begin{aligned}\vec{P}_1 &= \mathcal{N}(\vec{d}_{41}\rho_{41}^{(+)}e^{-i\omega_1 t} + \text{c.c.}) \\ &= (\chi_{41}\hat{e}_1\mathcal{E}_1e^{-i\omega_1 t} + \text{c.c.}),\end{aligned} \quad (11)$$

where \mathcal{N} is the density of the atomic medium. Now, Eqs. (10) and (11) will yield the linear response of the medium as

$$\chi_{41}(\Delta_1) = \frac{\mathcal{N}|d_{41}|^2}{\hbar}\rho_{41}^{(+)}. \quad (12)$$

The real and imaginary parts of the susceptibility χ_{41} in Eq. (12) gives the dispersion and absorption of the medium, respectively. The optical properties of the medium can be manipulated coherently by proper consideration of spatial shape and intensity of the different applied fields. The effect of different fields such as optical, microwave, and incoherent pump field on the medium properties are in sequence in the results and discussions section.

D. Beam propagation equation with paraxial approximation

The spatial dynamics of the probe and control fields along the z direction of the medium are governed by Maxwell's equations. The wave equation under the slowly varying envelope and paraxial wave approximations give the beam

propagation equation. The spatial evolution equations for the probe and control fields are obtained as

$$\frac{\partial g}{\partial z} = \frac{i}{2k_1} \left(\frac{\partial^2}{\partial x^2} + \frac{\partial^2}{\partial y^2} \right) g + 2i\pi k_1 \chi_{41} g, \quad (13a)$$

$$\frac{\partial G}{\partial z} = \frac{i}{2k_2} \left(\frac{\partial^2}{\partial x^2} + \frac{\partial^2}{\partial y^2} \right) G. \quad (13b)$$

The terms within the parentheses on the right-hand side of Eqs. (13a) and (13b) are related to transverse variation of the laser beam. These terms account for the diffraction either in free space or in the medium. The second term on the right-hand side of Eq. (13a) is responsible for the dispersion and absorption or gain of the probe beam. Note that the effects of the atomic coherences on the control beam propagation are very negligible under the weak probe field [27]. Therefore, we study the effect of both diffraction and dispersion for the spatial evolution of the probe beam, whereas we include only the effect of diffraction for the control beam dynamics.

III. RESULTS AND DISCUSSIONS

A. Susceptibility with homogeneous wave fields

We first study the atomic coherences by using homogeneous optical and microwave fields under the steady-state condition. The quantum interference of atomic coherences induces EIT, MIA, and LWI in our system. The characteristics of these quantum interference phenomena are illustrated in Fig. 2. In Fig. 2 we have plotted the variations of the imaginary part of the probe susceptibility with probe field detuning Δ_1 in the presence and absence of both microwave and

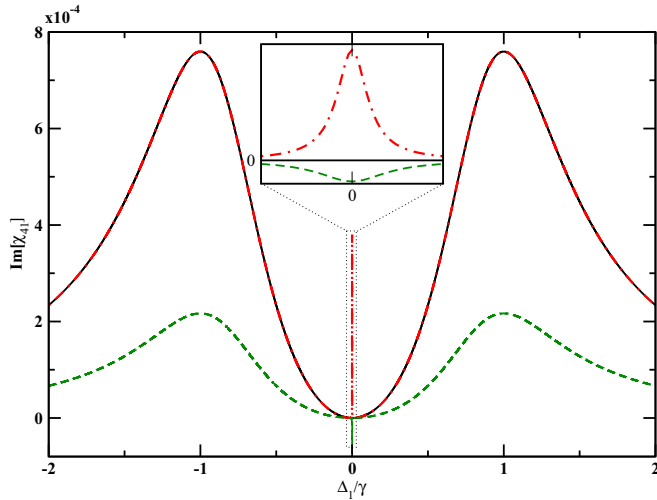


FIG. 2. (Color online) The variations of the imaginary part of the probe susceptibility with the detuning Δ_1 in the presence and absence of both microwave field and incoherent pump is plotted. The zoomed part of the absorption spectrum corresponding to medium loss, gain, or transparency at the line center is shown in the inset. The corresponding parameters for these regimes are $\Omega(x, y) = 0.01\gamma$, $r = 0$ (red dot-dashed line), $\Omega(x, y) = 0.01\gamma$, $r = 0.0005\gamma$ (green dashed line), and $\Omega(x, y) = 0\gamma$, $r = 0$ (black solid line). The common parameters are $G(x, y) = 1.0\gamma$, $\Delta_2 = \Delta_3 = 0$, $\Gamma = 0.0001\gamma$, $\gamma = 3\pi \times 10^6$ rad/s, $\lambda = 795$ nm, and $\mathcal{N} = 5 \times 10^{11}$ atoms/cm³.

incoherent pump fields. In the absence of both microwave and incoherent pump fields, the four-level system reduces to a three-level Λ system with a weak probe and a strong control field. The probability amplitudes of the two arms of the Λ system lead to destructive interference. This interference enables us to cancel the absorption of the probe field provided the two-photon resonance condition is fulfilled as shown in Fig. 2. This phenomenon is known as EIT. In EIT, a single transparency window is accompanied by two absorptive peaks which originate from the strong control field. Now this single transparency window can be split into double transparency windows by the use of the microwave field. It is clear from Fig. 2 that the double transparency window is accompanied by a very narrow absorption peak. This peak occurs due to the double dark states formed by the microwave field at three-photon resonance condition. Further, the position and width of these two transparency windows strongly depend on the intensity of the microwave field. Now a relatively weak incoherent pump acting along the probe transition can switch the absorption peak to a gain dip. The second term in the numerator of Eq. (10) is responsible for gain around the line center. This gain characteristic is illustrated by the green dashed line in Fig. 2. At three-photon resonance the second term is negative and larger than the first term which changes the properties of the medium from absorption into gain. Thus the presence of both weak microwave and incoherent pump fields is able to produce a gain window for the medium.

B. Susceptibility with inhomogeneous control field

In this section, we discuss the effect of a spatially inhomogeneous time independent field on the linear susceptibility given in Eq. (12). For this purpose, we change the control field profile from a spatially homogeneous field to a spatially inhomogeneous field while keeping the rest of the fields as spatially homogeneous for further study. The spatially inhomogeneous transverse profile of the control field is a combination of more than one Gaussian peak. At $z = 0$, the control beam can be written as

$$G(x, y) = G_0 \sum_{i=1}^n e^{-\{(x-a_i)^2 + y^2\}/w_c^2}, \quad (14)$$

where G_0 is the initial peak amplitude, w_c is the beam width, and a_i 's are the individual peak positions. The full width at half maximum of each individual peak is $\sqrt{2\ln 2}w_c$. Figure 3 shows the intensity distribution of the control field against radial position x at the entry face of the medium. The overlapping of two peaks gives rise to a central minimum with nonzero intensity as shown in Fig. 3. The Rayleigh-limited or Sparrow-limited control field images can be formed when the intensity of the peak normalized central minimum is $I_{\min} \sim 0.5$ or ~ 0.7 , respectively. The resolution of the diffraction-limited images can be improved by reducing the central minimum intensity to zero. Thus, by increasing the peak separation or by decreasing the width of the individual peak enables one to create a high-resolution image.

The spatially modulated control field perturbs the probe beam susceptibility along the transverse direction as shown in Fig. 4. Figure 4 illustrates the spatial variation of the real and imaginary parts of χ_{41} as a function of the transverse axis x

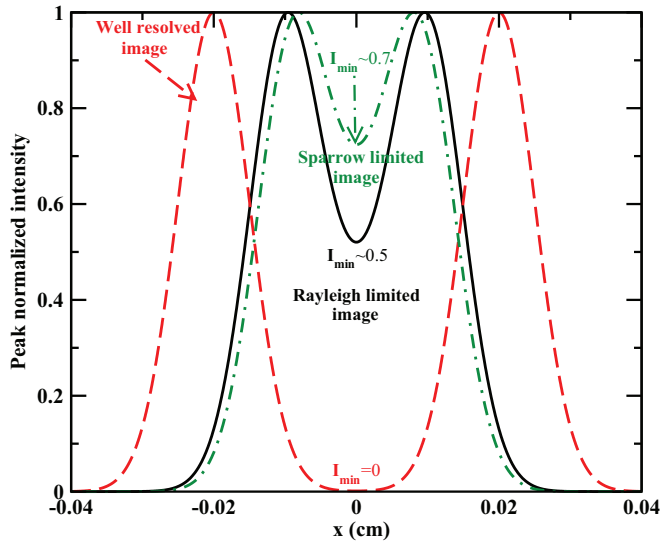


FIG. 3. (Color online) Spatial intensity variation of the control image is plotted against the transverse axis x with $y = 0$ at entry face of the vapor cell. The Rayleigh-limited and Sparrow-limited control images are formed by choosing $a_1 = -a_2 = 0.01$ cm and $a_1 = -a_2 = 0.009$ cm, respectively. The individual peaks can be well resolved by changing $a_1 = -a_2 = 0.02$ cm. The common parameters of the two graphs are $G_0 = 1\gamma$ and $w_c = 100 \mu\text{m}$.

for the $y = 0$ plane. A very special inhomogeneous character of dispersion ($\text{Re}[\chi_{41}]$) and absorption ($\text{Im}[\chi_{41}]$) causes the spatial modulation in phase and amplitude for the probe field, respectively. Since the phase of the probe beam is influenced by the copropagating control beam, this phase modulation is termed as cross phase modulation (XPM) [34]. The mutual coupling between the optical beams is attributed to XPM which causes focusing of the probe beam. The amplitude modulation results in attenuation or gain of the probe beam.

The curves of Fig. 4 represent three different cases of EIT, MIA, and LWI, respectively. It is clear from Fig. 4 that for the MIA and LWI cases two transparency windows are formed at higher intensity regions, whereas absorption occurs in relatively low intensity regions of control field G defined by two Gaussian modes using Eq. (14). The real part of the susceptibility is maximized at these higher intensity regions. This resembles two parallel waveguidelike structures with claddings ($0.0075 \text{ cm} \gtrsim |x| \gtrsim 0.0175 \text{ cm}$) and cores ($0.0175 \text{ cm} \gtrsim |x| \gtrsim 0.0075 \text{ cm}$). In order to have a perfect waveguiding, there should be a high contrast between core and cladding. In the case of EIT, it is evident from Fig. 4 that a single transparency window is formed and the variation in refractive index around $x = 0$ is very small. Therefore, the single transparency window has failed to create two parallel waveguides. As a result, EIT is not suitable to separate out the modes with high resolution. However, in the case of MIA, one can see a sharp variation in refractive index (red long-dashed line) around $x = 0$, with a rapid increase in contrast from core to cladding. But there is a reasonable increase in absorption in the region between $0.0175 \text{ cm} \gtrsim |x| \gtrsim 0.0075 \text{ cm}$ of the doublet as compared to EIT. This increment will reduce transmission of the probe beam and therefore, its visibility seems to be restricted.

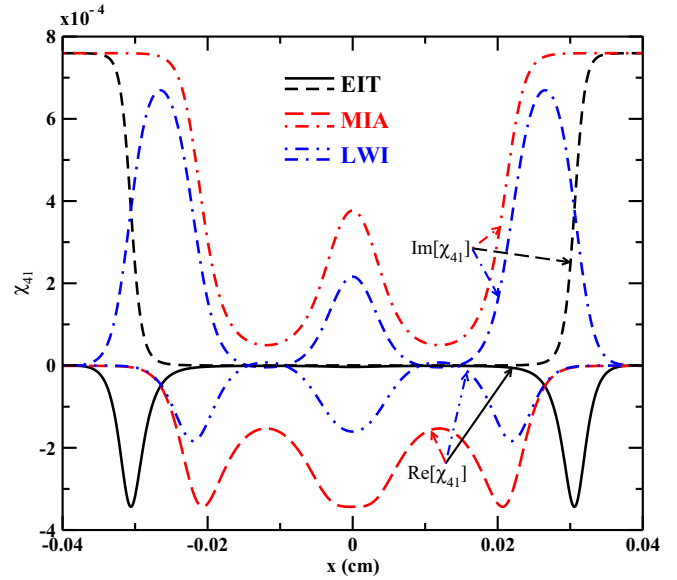


FIG. 4. (Color online) The spatial variation of the real ($\text{Re}[\chi_{41}]$) and imaginary ($\text{Im}[\chi_{41}]$) parts of χ_{41} . The plots are shown against the transverse axis coordinate x of the control beam for the $y = 0$ plane. The different curves are for three different sets of parameters: $\Omega(x, y) = 0.015\gamma$, $r = 0$, $\Delta_1 = 0.001\gamma$ (red, long-dashed and dot-dashed lines); $\Omega(x, y) = 0.015\gamma$, $r = 0.0005\gamma$, $\Delta_1 = 0.001\gamma$ (blue, dashed double-dot and dot double-dashed lines), and $\Omega(x, y) = 0$, $r = 0$, $\Delta_1 = -0.001\gamma$ (black, solid and short-dashed lines). The control beam parameters are $G_0 = 1\gamma$, $w_c = 100 \mu\text{m}$, and $a_1 = -a_2 = 0.012$ cm.

Interestingly, in the case of LWI, the refractive index contrast between core and cladding is higher than the other two cases. This contrast enhancement causes strong focusing of the probe beam towards the center of the two peaks of the control field. As a result the width of the probe beam becomes narrow, which can improve the contrast of the cloned image on the probe field. Also the two dips of the doublet changes from absorption into gain can produce the enhancement of the cloned beam transmission. Hence the weak probe beam is not only guided or focused but also amplified in order to preserve the information during the propagation through the optical medium. This is the key mechanism of cloning the unresolvable or just-resolvable control field profile to the probe field with high resolution. In the following, we use the inhomogeneous susceptibility for the LWI case to illustrate the improvement of the resolution of the optically cloned images of the control field onto the probe field.

C. Beam propagation dynamics

We numerically integrate the paraxial wave equations (13a) and (13b) by using a higher order split operator method [35] to study the propagation dynamics of both control and probe beams. First, we explore the cloning of the Rayleigh-limited control beam onto the probe beam in the presence of both microwave and incoherent pump fields. For this purpose, we set $w_c = 100 \mu\text{m}$ and $a_1 = -a_2 = 0.01$ cm in Eq. (14). The results for the spatial evolution of the control and the probe profiles throughout the medium are shown in Fig. 5. It is

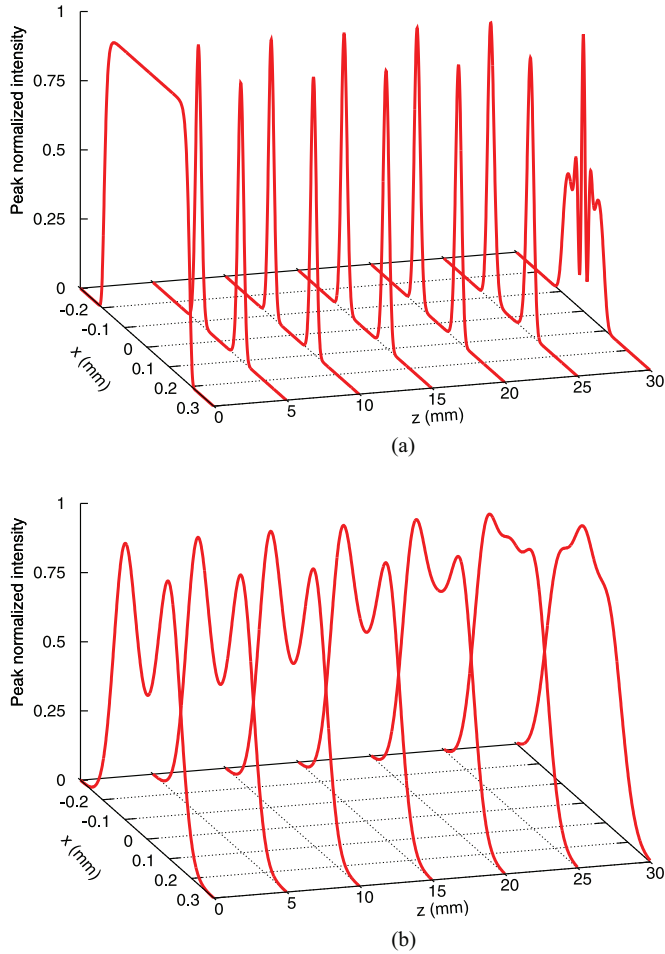


FIG. 5. (Color online) In panel (a), the spatial evolution of the probe beam profile is shown against the transverse coordinate x for the $y = 0$ plane at different propagation distances z . In panel (b), the peak-normalized intensity profile of the control beam is shown at different propagation distances z . The parameters are chosen as follows: $\Omega(x, y) = 0.018\gamma$, $r = 0.00075\gamma$, $\Delta_1 = 0.001\gamma$. The control beam (Rayleigh-limited) parameters are the same as in Fig. 3.

clear from Fig. 5(a) that within a very short distance, the control field structure is mapped onto the probe with central minimum reduced to zero. As a result, the finesse, which is the ratio of the spacing between peaks to the width of peaks of the transmitted probe beam at $z = 2.5$ cm, is four times smaller than the initial control beam finesse. The optically cloned probe image at $z = 2.5$ cm is well matched with the control field envelope expression (14) for the parameters $w_c = 29 \mu\text{m}$ and $a_1 = -a_2 = 0.01$ cm. We also find that the integrated transmission of the output probe beam at $z = 2.5$ cm is about 98%. The probe beam transmission can be changed by changing the incoherent pump field rate r . Figure 5(a) depicts the intensity profile of the control beam at different propagation distances z . We find that the shape of the control beam is gradually distorted due to diffraction as it propagates through the medium. As a consequence, control beam induced waveguide structure in the medium is modified. Accordingly the shape of the cloned beam starts experiencing diffraction

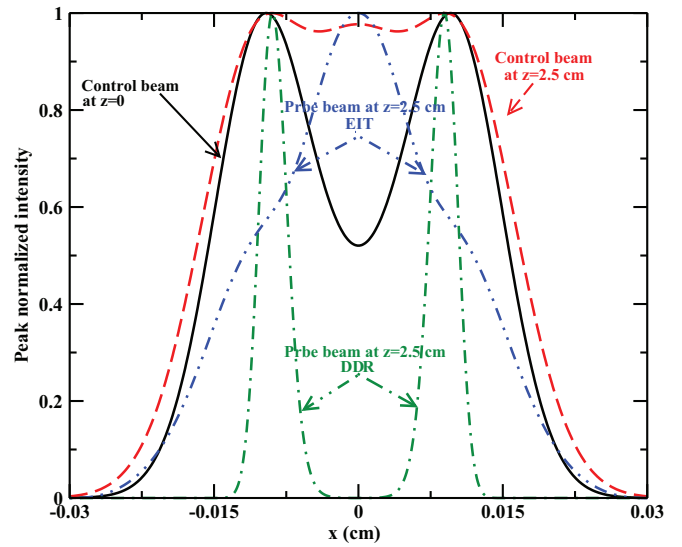


FIG. 6. (Color online) A comparison study of EIT and DDR with an incoherent pump for cloning of the just-resolved control images onto the probe beam at the output of the vapor cell with length $L = 2.5$ cm. The parameters are the same as in Fig. 4.

after $z = 2.5$ cm propagation distance as shown in Fig. 5(a). Long-distance diffractionless cloned image propagation can be achieved by considering a tightly focused control beam [12] or self-reconstructing Bessel control beam [36].

Figure 6 compares the cloning mechanism in the presence and absence of both microwave and incoherent pump fields. The Rayleigh-limited control field structure generated a double transparency window and a single transparency window for the DDR and EIT systems, respectively. It is clear from Fig. 6 that the double transparency window enabled perfect cloning of the control image with high resolution, whereas the single transparency window failed to clone the control image to the transmitted probe beam. We also notice that the DDR induced waveguide structure can support the propagation of the cloned probe beam without any diffraction. In contrast, for the EIT case, the transmitted probe beam suffers severe distortion due to the lack of a parallel waveguidelike structure inside the medium. Hence the EIT-based mechanism has a limitation to clone unresolved or just-resolved control images onto a probe beam without loss of generality.

Next, we demonstrate how the microwave and incoherent pump fields offer unprecedented control over the image cloning for unresolved images. For this purpose, we consider a more complex structure of control beam consisting of three Gaussian peaks. Figure 7 shows the radial distribution of the input Sparrow-limited control beam (at $z = 0$) and output probe beam at $z = 1$ cm. As in Fig. 7(b) it can be seen that the cloned probe images contain three distinguishable peaks even though the control beam profile is unresolved. Surprisingly, the integrated transmission intensity of the cloned probe image is approximately 74%. Thus microwave and incoherent pump fields allow one to clone the diffraction-limited control field image onto the probe beam with improved spatial resolution and high transmission. We also verified that the resolution enhancement of cloned images can be possible even for Rayleigh-limited control images with the Bessel as well as

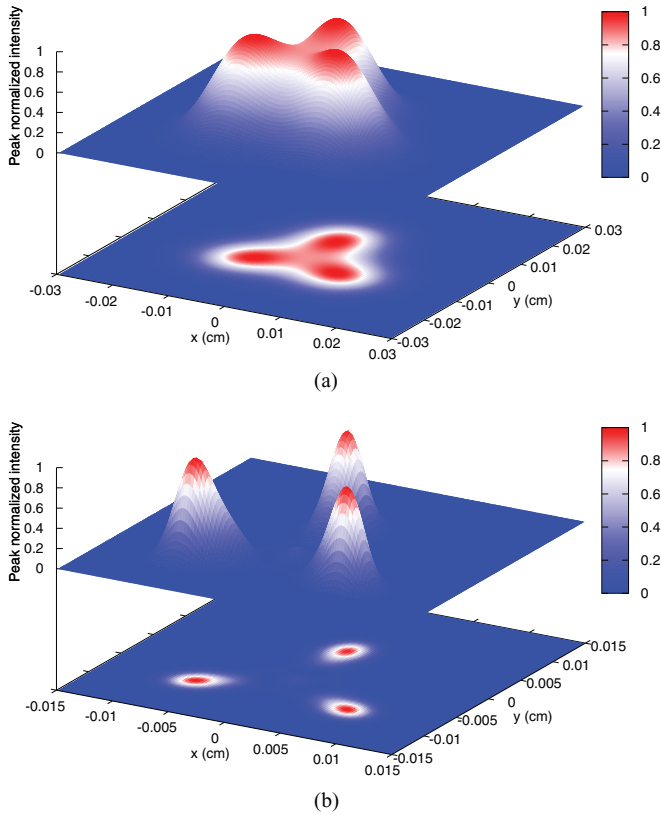


FIG. 7. (Color online) Picture (a) shows a three-dimensional intensity profile of the input control beam. Picture (b) shows the transmitted probe beam at the output of a 1-cm-long medium. The parameters are as in Fig. 5 except the locations of the three peaks are $(-0.009, -0.009)$, $(0.009, -0.009)$, and $(0.0, 0.0066)$ cm, $\Omega(x, y) = 0.02\gamma$, and $r = 0.00073\gamma$.

non-Gaussian shape. These studies may be useful for practical applicability such as optical microscopy, quantum metrology, and quantum imaging [37].

D. Spatial optical switching

Here, we show how the propagation dynamics of the probe beam can be controlled by switching the microwave field on and off. The well-resolved control beam image is being considered for this demonstration. The individual peak has a width $100 \mu\text{m}$ corresponding to a Rayleigh length of 4 cm. The spatially dependent control field assisted atomic waveguide can protect the features of the cloned beam in a 4-cm-long medium. Figure 8(a) illustrates that the nondiffracting cloned probe beam propagation is possible inside the medium in both the EIT and LWI systems. We found that the width and the transmission of the cloned beam at $z = 3$ cm are $25 \mu\text{m}$ ($100 \mu\text{m}$) and 60% (5%) for the LWI (EIT) mechanism. Therefore, the precise control of finesse and the contrast of the output cloned probe beam can be achieved by application of coherent fields and an incoherent pump field interacting in a four-level atomic medium. Figure 8(b) shows how the microwave-induced absorption can be utilized to attenuate the probe beam gradually inside the medium in the absence of an incoherent pump field. Thus, the microwave field which

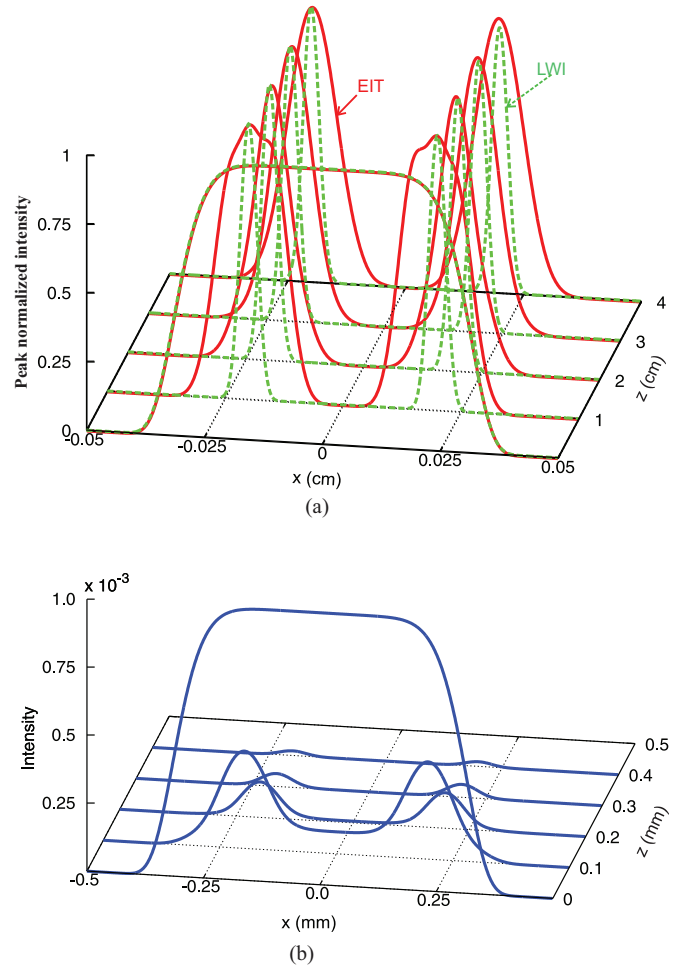


FIG. 8. (Color online) The intensity profile of the probe field transmission is shown against the transverse axis x with $y = 0$ at different propagation distances z . The top panel shows the probe beam is turned on in both the EIT and LWI cases. The lower panel shows the probe beam is turned off in the MIA situation. The initial profile of the control field contains two well-resolved Gaussian peaks with location $a_1 = -a_2 = 0.02$ cm as in Eq. (14). The parameters used in the different phenomena for spatial optical switching are as follows: in the EIT case [$\Omega(x, y) = 0, r = 0, \Delta_1 = -0.005\gamma$], in the LWI case [$\Omega(x, y) = 0.01\gamma, r = 0.0001\gamma, \Delta_1 = 0.0001\gamma$], and in the MIA case [$\Omega(x, y) = 0.01\gamma, r = 0, \Delta_1 = 0.0001\gamma$].

connects the lower level metastable states of a four-level system can switch off the probe beam propagation inside the medium. This investigation can be applicable for all optical switching and logic gates [33,38].

IV. CONCLUSION

In conclusion, we have revealed a scheme to improve the resolution of the cloned image based on the quantum interference effects induced by interacting dark resonances. For this purpose, we have used a four-level atomic system interacting with three coherent fields and an incoherent pump field. An atomic waveguide structure is formed inside the medium by using a spatially modulated control field. The refractive-index contrast between the core and cladding of

the atomic waveguide can be increased by the use of a sharp absorption peak associated with double dark resonances. The high contrast atomic waveguide enables us to imprint the Rayleigh- or Sparrow-limited control images to a probe field with high resolution. The transverse feature of the control image is efficiently cast onto the probe field even though the control image suffers distortion due to the diffraction during the propagation. Our numerical result shows that the propagation of a high-resolution cloned image is possible until the feature of the control image is lost completely. We used an

incoherent pump field in order to increase the transmission of the cloned probe image. Finally, we have also demonstrated that spatial optical switching is possible by the use of EIT, LWI, and MIA mechanisms.

ACKNOWLEDGMENTS

One of the authors (T.N.D) gratefully acknowledges funding by the Science and Engineering Board (Grant No. SR/S2/LOP-0033/2010).

APPENDIX: COEFFICIENTS FOR STEADY-STATE SUSCEPTIBILITY

$$\rho_{11}^{(0)} = \frac{[2(r + \gamma)|G|^2\Omega^2\{\gamma(\Gamma\gamma + |G|^2) + \Gamma[(\Delta_2 + \Delta_3)^2 + \Omega^2]\}]}{D}, \quad (\text{A1})$$

$$\rho_{22}^{(0)} = [r\gamma|G|^6 + |G|^4(2\Gamma\gamma^2 - 2\gamma\Delta_2\Delta_3 - 2\gamma\Delta_3^2 + \Gamma\Omega^2 - \gamma\Omega^2) + 2\Gamma\Omega^2[\Delta_2^4 + 2\Delta_2^3\Delta_3 + \gamma^2\Delta_3^2 + \Delta_2^2(2\gamma^2 + \Delta_3^2 - 2\Omega^2) + 2\Delta_2\Delta_3(\gamma^2 - \Omega^2) + (\gamma^2 + \Omega^2)^2] + |G|^2\{\gamma\Delta_3^4 + (\gamma^2 + \Omega^2)[\Gamma^2\gamma - (\Gamma - 2\gamma)\Omega^2] + \Delta_3^2[\gamma(\Gamma^2 + \gamma^2) + 2(\Gamma + 2\gamma)\Omega^2] + \Delta_2^2[\Gamma^2\gamma + \gamma\Delta_3^2 + (5\Gamma + 2\gamma)\Omega^2] + \Delta_2\Delta_3[2\Gamma^2\gamma + 2\gamma\Delta_3^2 + (7\Gamma + 6\gamma)\Omega^2]\}]/D, \quad (\text{A2})$$

$$\rho_{33}^{(0)} = (r\Omega^2\{2\Gamma\Delta_2^4 + 4\Gamma\Delta_2^3\Delta_3 + \Delta_3^2[2\Gamma\gamma^2 + (2\Gamma + \gamma)|G|^2] + \Delta_2^2[2\Gamma\Delta_3^2 + (3\Gamma + 2\gamma)|G|^2 + 4\Gamma(\gamma^2 - \Omega^2)] + \Delta_2\Delta_3[(5\Gamma + 2\gamma)|G|^2 + 4\Gamma(\gamma^2 - \Omega^2)] + [|G|^2 + 2(\gamma^2 + \Omega^2)][\gamma|G|^2 + \Gamma(\gamma^2 + \Omega^2)]\})/D, \quad (\text{A3})$$

$$\rho_{44}^{(0)} = \frac{(2r|G|^2\Omega^2\{\gamma(\Gamma\gamma + |G|^2) + \Gamma[(\Delta_2 + \Delta_3)^2 + \Omega^2]\})}{D}, \quad (\text{A4})$$

$$D = (r\gamma|G|^6 + |G|^4\{2r\gamma[\Gamma\gamma - \Delta_3(\Delta_2 + \Delta_3)] + [2\gamma^2 + r(\Gamma + 4\gamma)]\Omega^2\} + 4r\Gamma\Omega^2\{(\gamma^2 + \Delta_2^2)[\gamma^2 + (\Delta_2 + \Delta_3)^2] + 2[\gamma^2 - \Delta_2(\Delta_2 + \Delta_3)]\Omega^2 + \Omega^4\} + |G|^2\{r\gamma(\Gamma^2 + \Delta_3^2)[\gamma^2 + (\Delta_2 + \Delta_3)^2] + \{\gamma[2\Gamma\gamma^2 + r(\Gamma + 2\gamma)^2] + 2[\Gamma\gamma + 2r(3\Gamma + \gamma)]\Delta_2^2 + 4(5r\Gamma + 2r\gamma + \Gamma\gamma)\Delta_2\Delta_3 + (8r\Gamma + 5r\gamma + 2\Gamma\gamma)\Delta_3^2\}\Omega^2 + 2[\Gamma\gamma + 2r(\gamma + \Gamma)]\Omega^4\}). \quad (\text{A5})$$

-
- [1] Lord Rayleigh, *Philos. Mag.* **8**, 261 (1879).
[2] B. A. A. Saleh and M. C. Teich, *Fundamentals of Photonics* (Wiley, New York, 1991).
[3] M. Born and E. Wolf, *Principles of Optics* (Cambridge University Press, Cambridge, England, 1999).
[4] E. Arimondo, *Prog. Opt.* **35**, 257 (1996).
[5] S. E. Harris, *Phys. Today* **50**, 36 (1997).
[6] M. Fleischhauer, A. Imamoglu, and J. P. Marangos, *Rev. Mod. Phys.* **77**, 633 (2005).
[7] O. Kocharovskaya, *Phys. Rep.* **219**, 175 (1992).
[8] T. W. Hansch, M. D. Levenson, and A. L. Schawlow, *Phys. Rev. Lett.* **26**, 946 (1971).
[9] G. S. Agarwal and T. N. Dey, *Laser Photonics Rev.* **3**, 287 (2009).
[10] A. G. Truscott, M. E. J. Friese, N. R. Heckenberg, and H. Rubinsztein-Dunlop, *Phys. Rev. Lett.* **82**, 1438 (1999).
[11] R. Kapoor and G. S. Agarwal, *Phys. Rev. A* **61**, 053818 (2000).
[12] P. K. Vudiyasetu, D. J. Starling, and J. C. Howell, *Phys. Rev. Lett.* **102**, 123602 (2009).
[13] T. N. Dey and J. Evers, *Phys. Rev. A* **84**, 043842 (2011).
[14] R. R. Moseley, S. Shepherd, D. J. Fulton, B. D. Sinclair, and M. H. Dunn, *Phys. Rev. Lett.* **74**, 670 (1995).
[15] R. R. Moseley, S. Shepherd, D. J. Fulton, B. D. Sinclair, and M. H. Dunn, *Phys. Rev. A* **53**, 408 (1996).
[16] D. R. Walker, D. D. Yavuz, M. Y. Shverdin, G. Y. Yin, A. V. Sokolov, and S. E. Harris, *Opt. Lett.* **27**, 2094 (2002).
[17] N. A. Proite, B. E. Unks, J. T. Green, and D. D. Yavuz, *Phys. Rev. A* **77**, 023819 (2008).
[18] M. Mitsunaga, M. Yamashita, and H. Inoue, *Phys. Rev. A* **62**, 013817 (2000).
[19] D. Bortman-Arbiv, A. D. Wilson-Gordon, and H. Friedmann, *Phys. Rev. A* **63**, 031801(R) (2001).
[20] J. Cheng and S. Han, *Opt. Lett.* **32**, 1162 (2007).
[21] V. A. Sautenkov, H. Li, Y. V. Rostovtsev, and M. O. Scully, *Phys. Rev. A* **81**, 063824 (2010).

- [22] L. Zhang, T. N. Dey, and J. Evers, *Phys. Rev. A* **87**, 043842 (2013).
- [23] O. Firstenberg, M. Shuker, N. Davidson, and A. Ron, *Phys. Rev. Lett.* **102**, 043601 (2009).
- [24] O. Firstenberg, P. London, M. Shuker, A. Ron, and N. Davidson, *Nat. Phys.* **5**, 665 (2009).
- [25] O. Firstenberg, M. Shuker, A. Ron, and N. Davidson, *Rev. Mod. Phys.* **85**, 941 (2013).
- [26] H. Li, V. A. Sautenkov, M. M. Kash, A. V. Sokolov, G. R. Welch, Y. V. Rostovtsev, M. S. Zubairy, and M. O. Scully, *Phys. Rev. A* **78**, 013803 (2008).
- [27] O. N. Verma, L. Zhang, J. Evers, and T. N. Dey, *Phys. Rev. A* **88**, 013810 (2013).
- [28] C. O'Brien and O. Kocharovskaya, *Phys. Rev. Lett.* **107**, 137401 (2011).
- [29] M. D. Lukin, S. F. Yelin, M. Fleischhauer, and M. O. Scully, *Phys. Rev. A* **60**, 3225 (1999).
- [30] Y. C. Chen, Y. A. Liao, H. Y. Chiu, J. J. Su, and I. A. Yu, *Phys. Rev. A* **64**, 053806 (2001).
- [31] S. F. Yelin, V. A. Sautenkov, M. M. Kash, G. R. Welch, and M. D. Lukin, *Phys. Rev. A* **68**, 063801 (2003).
- [32] C. Y. Ye, A. S. Zibrov, Y. V. Rostovtsev, and M. O. Scully, *Phys. Rev. A* **65**, 043805 (2002).
- [33] H. Wang and X. Peng, *J. Opt. Soc. Am. B* **29**, 429 (2012).
- [34] G. P. Agrawal, *Phys. Rev. Lett.* **64**, 2487 (1990).
- [35] A. D. Bandrauk and H. Shen, *J. Phys. A: Math. Gen.* **27**, 7147 (1994).
- [36] F. O. Fahrbach and A. Rohrbach, *Nat. Commun.* **3**, 632 (2012).
- [37] C. A. Mack, *Fundamental Principles of Optical Lithography: The Science of Microfabrication* (Wiley, West Sussex, England, 2007); R. T. Glasser, H. Cable, J. P. Dowling, F. De Martini, F. Sciarrino, and C. Vitelli, *Phys. Rev. A* **78**, 012339 (2008); V. Giovannetti, S. Lloyd, L. Maccone, and J. H. Shapiro, *ibid.* **79**, 013827 (2009).
- [38] Z. Nie, H. Zheng, Y. Zhang, Y. Zhao, C. Zuo, C. Li, H. Chang, and M. Xiao, *Opt. Express* **18**, 899 (2010).